Cyclic synchronous patterns in coupled discontinuous maps

Keli Yang,[1,2,3] Xingang Wang,[1,2] and Shi-Xian Qu[1,2,*]
[1]*Institute of Theoretical & Computational Physics, Shaanxi Normal University, Xi'an 710062, China*
[2]*School of Physics and Information Technology, Shaanxi Normal University, Xi'an 710062, China*
[3]*Nonlinear Research Institute, Baoji University of Arts and Sciences, Baoji 721016, China*
(Received 11 December 2014; published 12 August 2015)

Cyclic collective behaviors are commonly observed in biological and neuronal systems, yet the dynamical origins remain unclear. Here, by models of coupled discontinuous map lattices, we investigate the cyclic collective behaviors by means of cluster synchronization. Specifically, we study the synchronization behaviors in lattices of coupled periodic piecewise-linear maps and find that in the nonsynchronous regime the maps can be synchronized into different clusters and, as the system evolves, the synchronous clusters compete with each other and present the recurring process of cluster expanding, shrinking, and switching, i.e., showing the cyclic synchronous patterns. The dynamical mechanisms of cyclic synchronous patterns are explored, and the crucial roles of basin distribution are revealed. Moreover, due to the discontinuity feature of the map, the cyclic patterns are found to be very sensitive to the system initial conditions and parameters, based on which we further propose an efficient method for controlling the cyclic synchronous patterns.

DOI: 10.1103/PhysRevE.92.022905 PACS number(s): 05.45.Xt

I. INTRODUCTION

Cyclic collective behaviors refer to the spontaneous, repeated switching of the system dynamics among different operating modes (patterns), which have been widely observed in ecological, biological, and neuronal systems, and are believed to be crucial for many of the system functions [1]. A well-known example is the cyclic alternating pattern occurring in sleep, where the brain activities are found to be switching recurringly between different stages characterized by distinct electroencephalography features, namely, the sleep cycles [2]. Another example of cyclic behavior is the gait switching in animal locomotion, in which the muscle activities are changing versatilely among different motor patterns, as depicted by the electromyography signals [3]. For its significant implications to the system functions, e.g., the role of sleep cycles in learning and memory [4], as well as to the artificial intelligence, e.g., the design of working machines and robots [5], cyclic collective behaviors have been extensively studied by researchers from different fields in the past years. In the theoretical studies of cyclic behaviors, one important approach has been modeling the switching of patterns in systems of coupled nonlinear oscillators [6–11]. For instance, in Ref. [6], a simple model of coupled phase oscillators has been proposed to explore the sleep-wake rhythm in human circadian system, with the theoretical results in good agreement with the experimental data, and in Ref. [7], by the model of coupled nonlinear oscillators, gait patterns similar to that of human being have been generated, based on which a two-legged walking machine of locomotive activities has been designed. It should be pointed out that in all these studies, the switching of the patterns relies on the external control signals (e.g., resetting the oscillator states or changing the system parameters), and it remains a challenge to generate cyclic pattern in autonomous systems (e.g., the sleep cycle) [7–10,12,13].

A kind of collective behaviors that are commonly observed in coupled nonlinear oscillators is synchronization, which has attracted continuous interest in nonlinear science [14–16]. In the general picture of synchronization, the (periodic or chaotic) motions of all the coupled oscillators are confined to the same trajectory in the phase space when the coupling strength among the oscillators is larger to some critical value, knowing as the state of complete synchronization [15]. Depending on the way how the motions are correlated, different types of synchronization can be realized, e.g., phase synchronization, generalized synchronization, lag synchronization, etc. [17]. Recently, stimulated by the discoveries of the small-world and scale-free features in many natural and man-made systems [18,19], a new surge of research has appeared in the synchronization studies, in which the important roles of network structure on synchronization have been revealed [20–23]. Besides the state of global synchronization, partial (cluster) synchronization has been also broadly interested and extensively studied, for its strong connections to the functioning of many biological and physiological systems [24–26]. In a partial synchronization state, the oscillators are synchronized into different clusters, forming the synchronous patterns. Within each cluster, the motions of the oscillators are highly correlated, while oscillators in different clusters are loosely or not correlated. Very recently, partial synchronization in networks beyond regular structures has been investigated, e.g., regular networks with shortcut links and complex networks [12,13,27–30]. Still, without the help of control signals, the system dynamics cannot be switched automatically between different synchronous patterns [10,12]. (Please note that while competition of synchronous clusters may occur during the transient process of network synchronization, it should not be regarded as an example of pattern switching of interest here, as the system will be finally stabilized onto a stationary pattern, e.g., the state of global synchronization [13,31].)

For its rich phenomenology and computational efficiency, the model of coupled map lattice (CML) has been widely used in the literature for exploring the collective behaviors in systems of coupled nonlinear oscillators, including

*Corresponding author: sxqu@snnu.edu.cn

spatiotemporal chaos (chemical turbulence), pattern formation, synchronization, etc. [32]. In particular, distinct synchronous patterns have been observed in CML for different coupling structures, and rich phenomena of pattern formation have been observed [33–35]. According to the spatial behaviors of CML, the synchronous patterns can be roughly divided into two types: stationary and nonstationary. In a stationary pattern (also known as frozen pattern), once the pattern is formed, the contents of each synchronous cluster will be fixed during the system evolution [35–37]. In contrast, in a nonstationary pattern the contents of the synchronous clusters are varying with time, presenting the interesting phenomena of pattern evolution and competition [38–41]. One typical example of nonstationary pattern observed in CML is the traveling waves (fronts), in which the boundaries of the synchronous clusters (the interface of two neighboring homogeneous phases) are propagating on the lattices with some well-defined velocities [40,41]. When two traveling waves collide, the system dynamics might be switched to a new pattern form, e.g., the transition from partial to global synchronization. This kind of pattern switching, however, is not sustainable (it occurs only during the transient process of system evolution) and irregular (presents the complex interfacial dynamics) [39,41] and therefore is different from the cyclic patterns in which we are interested [1–3].

In the present work, we shall employ the lattices of coupled piecewise-linear maps to demonstrate the formation of cyclic synchronous patterns (in Sec. II), investigating the dynamical properties, analyzing the underlying mechanisms (in Sec. III), and proposing new methods for controlling them (in Sec. IV). Discontinuous map characterizes the motion for a variety of practical systems, such as nerve cells, electronic circuits, relaxation oscillators, and impact oscillators, and offers rich dynamical phenomena when an assembly of such maps are coupled [42–48]. Our studies of coupled piecewise-linear maps show that, given the local map is periodic and the basins of the attractors are continuously distributed (with nonfractal basin boundary), cyclic synchronous patterns in general can be generated by tuning the coupling strength. Moreover, due to the discontinuity feature of the piecewise-linear map, it is found that the cyclic synchronous pattern is very sensitive to the system initial conditions and coupling strength, making it feasible to control (alter) the pattern by very small perturbations. The findings shed light on the collective behaviors of coupled discontinuous maps and might be helpful in the understanding of the cyclic collective behaviors observed in biological and neuronal systems [1–5].

II. MODEL AND PHENOMENA

Our model of coupled piecewise-linear maps reads [39,49]

$$x_i(n+1) = (1-\varepsilon) f(x_i(n)) + \frac{\varepsilon}{2}[f(x_{i+1}(n)) + f(x_{i-1}(n))], \tag{1}$$

with n the discrete time, $i = 1, \ldots, N$ the map index, and ε the uniform coupling strength. The map in its isolated form is described as $x(n+1) = f(x(n))$, which, for the sake of simplicity, is set to be identical in the system. Each map is coupled to its nearest neighbors on a ring-structure lattice, i.e., with the periodic boundary condition, $x_1(n) = x_{N+1}(n)$. The piecewise-linear map has the form [50]

$$f(x) = \begin{cases} ax, & x < x_g, \\ b, & x \geqslant x_g, \end{cases} \tag{2}$$

with $x \in (0,1)$, $x_g = 1/a$, and a, b the bifurcation parameters. This map is a discrete version of the differential Chay model used widely in computational neuroscience and is able to generate the similar bifurcation scenario of the interspike interval observed in neural experiments (more details about the theoretical derivation and experimental realization of this map can be found in Ref. [50]). In particular, by the parameters $a = 2.5$ and $b = 0.1$, the isolated map has a superstable period-three orbit: $x_1^* = b = A$, $x_2^* = ab = B$, and $x_3^* = a^2 b = C$. Under the third-order composed map $f^3(x)$, the period-three orbit will be transferred into three fixed points (A, B, and C), with each point attracting an ensemble of initial conditions in the phase space. Different from the other types of nonlinear maps, e.g., the logistic map, here the attracting basins of the three fixed points are continuously distributed in the phase space. Specifically, within the interested interval $x \in (f^{-2}(x_g), 1)$ the attracting basins for A, B, and C are, respectively, $(f^{-2}(x_g), f^{-1}(x_g))$, $(f^{-1}(x_g), x_g)$ and $(x_g, 1)$, with $f^{-m}(x_g)$ the m-time backward image of the discontinuous point x_g. [The attracting basins in the interval $x \in (0, f^{-2}(x_g))$ are still continuously distributed, but in a hierarchical order; e.g., the basin of A is a combination of the intervals $(f^{-3k-2}(x_g), f^{-3k-1}(x_g))$, with $k = 1,2,3, \ldots, \infty$.] In our studies, we shall employ this period-three orbit as the local dynamics and investigate the collective behaviors of the lattices.

Setting $N = 100$ and $\varepsilon = 0.39$, we plot in Fig. 1(a) the system evolution started from a set of random initial

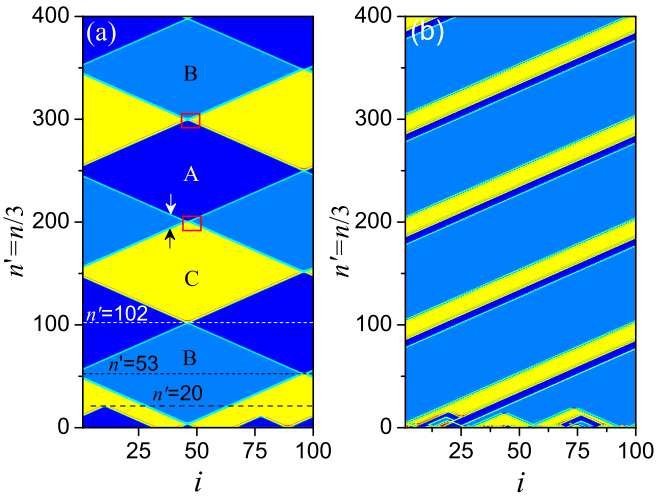

FIG. 1. (Color online) For the lattice of $N = 100$ coupled piecewise-linear maps and by the coupling strength $\varepsilon = 0.39$, the system evolutions under two different sets of initial conditions. (a) The formation of cyclic synchronous pattern, which has the period $T = 888$. (b) The formation of traveling synchronous pattern. The map states are recorded every three iterations, $n' = n/3$. The fixed points A, B, and C are represented by the dark (blue), gray (cyan), and light (yellow) colors, respectively. Arrows and rectangles in (a) mark, respectively, the processes of cluster competitions and interface collisions, which will be analyzed in detail in Figs. 2 and 3.

conditions. Here, to better present the synchronous patterns, Fig. 1 is plotted by the third-order composed map ($n' = n/3$); i.e., the map states are recorded every three iterations. Furthermore, to distinguish the synchronous clusters, we denote the A cluster, B cluster, and C cluster as the clusters staying on the fixed points A, B, and C, respectively. In Fig. 1(a), it is seen that the maps are quickly synchronized into a number of small clusters ($n' \approx 10$), and, as time increases, the small clusters compete with each other and are gradually combined into several large clusters ($n' \approx 20$), with a small B cluster in the middle ($32 \leqslant i \leqslant 62$). After that, the size of the B cluster is gradually enlarged by consuming other clusters, and, by the moment $n' \approx 53$, the system is dominated by the B cluster except several maps near the boundaries ($i = 96,97,98$). So far, this scenario of cluster combination is similar to that of transient synchronization observed in conventional studies [17,23]. (In the conventional picture of transient synchronization, as time increases, the few nonsynchronous maps will be also absorbed into the giant cluster, leading finally to the state of global synchronization.) However, in Fig. 1(a) it is seen that, instead of being absorbed to the giant B cluster, the few survived maps (the remnants of the C cluster) synchronize and form a small A cluster, which, during the following system evolution, is gradually expanded by consuming the B cluster. The expansion of the A cluster is stopped at $n' \approx 102$, where the system is dominated by the A cluster except several maps ($i = 45,46,47$). Then, just like what happens at $n' \approx 53$, the few survived maps synchronize and form a small C cluster, which starts to consume the A cluster. As shown in Fig. 1(a), this process of cluster competition is occurring repeatedly in a cyclic fashion: A cluster $\rightarrow$ B cluster $\rightarrow$ C cluster $\rightarrow$ A cluster. More specifically, after each period of $T = 888$ iterations, the system returns to exactly the same synchronous pattern; i.e., a cyclic synchronous pattern is generated.

The cyclic synchronous pattern shown in Fig. 1(a) is distinguished from other synchronous patterns in several aspects. First, different from the case of partial synchronization [35–37], in a cyclic pattern the size of the synchronous clusters is changing with time; i.e., the pattern is nonstationary. Specifically, during the process of cluster competition, the cluster interface (the thin layer between two neighboring clusters) is moving with a constant speed (the exact speed is determined by the clusters and the coupling strength, which will be discussed in detail later). Second, unlike the case of traveling wave in which the collision of the cluster interfaces finally leads to the state of global synchronization [39,41], in a cyclic pattern a small new cluster is born each time when two cluster interfaces collide. During the following evolution of the system, the new cluster "counterattacks" and consumes the giant cluster formed earlier. This feature of interface crossover is crucial for a cyclic pattern, as it continues the competition of synchronous clusters. Finally, the cyclic pattern in Fig. 1(a) is very sensitive to the system initial conditions and coupling strength. This feature is partially reflected in Fig. 1(b), in which the same system is started from another set of random initial conditions. It is seen that after a short transient period, the system is stabilized onto a traveling pattern. Regarding the above new features of a cyclic pattern, it is natural to ask the following questions: (1) why the synchronous pattern is nonstationary, i.e., the size of the synchronous clusters is changing with time; (2) how could the collision of two cluster interfaces give rise to a new cluster; and (3) why the system dynamics is sensitive to the initial conditions and coupling strength. To answer these questions, a detailed analysis of the dynamical properties of the cyclic pattern is necessary.

III. MECHANISM ANALYSIS

Before going to the detail analysis, we first give a brief discussion of the motion of the maps. Rewriting Eq. (1) as

$$x_i(n+1) = f(x_i(n)) + \Delta_i(n,\varepsilon), \tag{3}$$

it is straightforward to see that the motion of a map is jointly determined by two factors: the isolated map function, $f_i(x)$, and the coupling perturbation, $\Delta_i(n,\varepsilon) = \varepsilon[f(x_{i+1}(n)) + f(x_{i-1}(n)) - 2f(x_i(n))]/2$. While the former tends to constrain the map to the predefined trajectory (e.g., the period-three orbit adopted in the present work), the latter prevents this tendency by proving a perturbation. As $\Delta = 0$ for maps inside a cluster, only maps at the boundaries of the clusters are perturbed. This property makes the system dynamics characterized essentially by maps in the boundary regions. For such a boundary map, the perturbation it receives from the neighbors is timely varying. If at some instant of the system evolution a large perturbation occurs, then this map might "jump" to a new basin and be attracted to a new attractor, resulting in a modification of the cluster boundary. Otherwise, if the perturbation is small, the map will be staying around its original orbit, making the clusters stationary. Therefore, the evolution of the synchronous patterns can be interpreted as a competition between the map function and the coupling perturbations. In what follows, we try to interpret the observed phenomena from this viewpoint.

A. Cluster competition

We start by analyzing the nonstationary feature of the pattern, i.e., the dynamical process of cluster competition. To investigate, we monitor the evolution of the cluster interface, checking how a map is transferred from one cluster to another. Focusing on a short segment of the lattice, $i \in [26,46]$, we plot in Fig. 2(a) a succession of snapshots of the map states, which shows in detail how the 38th map is transferred from the C cluster to the B cluster as time increases. Initially ($n = 570$), the 38th map is located at the leftmost side of the C cluster. Then, driven by its left-side neighbor, the map is slightly diverged from C ($n = 573$), and from then on it escapes from the C cluster. In transferring to the B cluster, it is seen that the 38th map is first oscillating around C for a short period ($573 < n < 576$), then at $n = 579$ it is suddenly jumped to the neighboring region of B. After that, the map begins to oscillate around B. Finally, at $n = 588$, it is stabilized onto B and staying in the B cluster ever since. This process of cluster transition continues in a cyclic fashion. That is, after each period of $T' = 18$, a map in the C cluster will be transferred to the B cluster. Correspondingly, there are totally $L = T'/3 = 6$ maps in the transition region, which form the cluster interface.

The above process of cluster competition is more clearly presented in Fig. 2(b), in which the state of the 38th map is

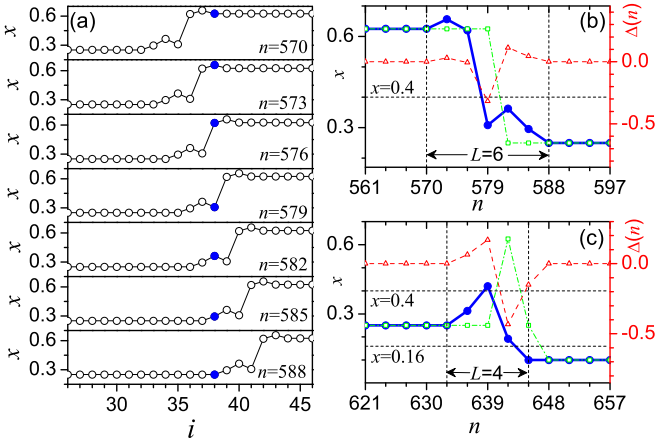

FIG. 2. (Color online) For the cyclic pattern shown in Fig. 1(a), the competitions of the synchronous clusters at places marked by the arrows. (a) Successive snapshots for a short segment of the lattice, $i \in [26,46]$, in which the 38th map (solid circles) is transferred from the C cluster to the B cluster after $T' = 18$ iterations. (b) The trajectory of the 38th map during its transition from the C to B cluster. The width of the cluster interface is $L = 6$. (c) The trajectory of the 38th map during its transition from the B to A cluster. The width of the cluster interface is $L = 5$. (b) and (c) The time evolutions of the isolated map (open squares) and the coupling perturbation $\Delta(n)$ (open triangles) are also presented as the references. The horizontal axes, $x = 0.4$ and $x = 0.16$, denote the basin boundaries.

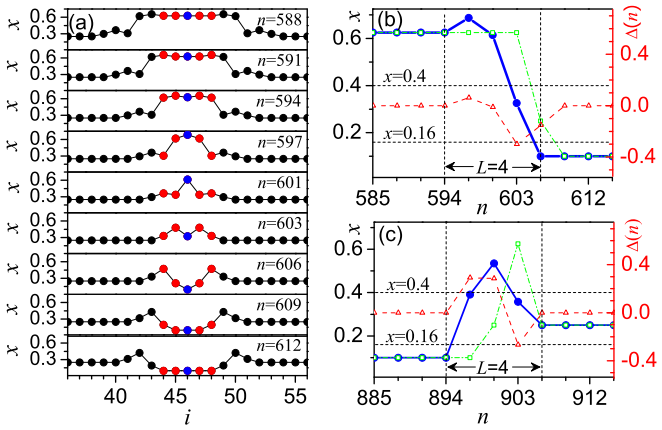

FIG. 3. (Color online) For the cyclic pattern shown in Fig. 1(a), the collisions of two counterpropagating cluster interfaces in the regions marked by rectangles. (a) Successive snapshots for a segment of the lattice, $i \in [36,56]$, during which the C cluster vanishes and an A cluster is newly born. (b) The trajectory of the 46th map during the process of interface collision. (c) The trajectory of the 46th map during the process of interface collision (the interfaces between the C and A cluster), which leads to the birth of a B cluster. As references, the time evolutions of the isolated map (open squares) and the coupling perturbation $\Delta(n)$ (right scale, open triangles) are also plotted in (b) and (c).

plotted as a function of time. To demonstrate the competition between the local map dynamics and the coupling perturbation, we present in Fig. 2(b) also the trajectory of the isolated map (the open squares) and the time evolution of coupling perturbation $\Delta(n)$ (the open triangles). The axis at $x = x_g = 0.4$ marks the boundary separating the basins of B and C. It is seen that at the critical moment $n = 579$, a large perturbation is generated, and, as a consequence, the map trajectory crosses the basin boundary $x = 0.4$. Specifically, the map jumps out from the basin of C and enters the basin of B. Combining the competition relationship described at the beginning of this section, the picture of cluster competition now is clear. Before the critical moment ($n < 579$), because C is a superstable fixed point and the coupling perturbation is very small, the map evolution is more influenced by the local dynamics than the couplings received from the neighboring maps. As a result, the map is confined to be oscillating around C. At the critical moment, the coupling perturbation is large enough to pull the map to the basin of B. After that, the map evolution is no longer influenced by C, but governed by the stable manifold of B. As in the following evolution the coupling perturbation is too small to push the trajectory out of the basin of B, and the map hence is staying within the same basin and is quickly stabilized onto B. This picture of cluster competition implies that, to make a map being successfully transferred from one cluster to another, two conditions are necessary: (1) a large coupling perturbation (to realize the basin crossing) and (2) the continuously distributed basins of the attractors (to make sure the map can be quickly stabilized in the new basin).

Basin crossing, however, does not always lead to the map transition. To show an example, in Fig. 2(c) we plot the trajectory of the 38th map for the period $621 \leqslant n \leqslant 657$, during which the A cluster is enlarged by one map by consuming the B cluster [see the cyclic pattern plotted in Fig. 1(a) for more details on the competition relationship between the A and B clusters]. Here it is observed that, during the map evolution, the map trajectory visits all the three basins, but it finally joins the A cluster. Here, although at the instant $n = 639$ the map crosses the boundary $x = 0.4$ and enters the basin of C, it is not attracted to C. Instead, it returns to the basin of A in the next iteration. In contrast, when it crosses the basin boundary $x = 0.16$ at $n = 645$, the map is immediately attracted to A and stays in the A cluster after that. The exceptional case occurring at $n = 639$ thus confirms that basin crossing is only a necessary, but not sufficient, condition for map transition.

B. Cluster collision

We next study the collision of two cluster interfaces. Successive snapshots for the maps $36 \leqslant i \leqslant 56$ are plotted in Fig. 3(a), which gives the details on what happens during the collision of two interfaces [this figure is a zoom-in plot for the rectangle region marked in Fig. 1(a) around $n' = 200$]. It is seen that initially ($n = 588$) the segment consists of three clusters, with the C cluster in the middle and two B clusters on the sides (actually the two B clusters here belong to the same cluster due to the periodic boundary condition). Then, with the increasing of time the C cluster is gradually shrunk, while the B clusters are enlarged. This process of cluster competition is similar to that of Fig. 2(a). By the moment $n = 594$, there is only one map, $i = 46$, left in the C cluster. Instead of being absorbed to the B cluster, it is found that after several iterations this map is attracted to A ($n = 606$). Then, very interestingly, the 46th map becomes the "seed" of a new cluster, the A cluster, which is gradually enlarged by consuming the B cluster in the following evolution.

A significant finding in Fig. 3(a) is the birth of the A cluster, which prevents the system from reaching the global synchronization state, and therefore maintaining the process of cluster competition. To have more details on the birth of this new cluster, we plot in Fig. 3(b) the trajectory of the 46th map, the central map in the C cluster, during the process of interface collision. It is seen that in its transition from C to A, the trajectory crosses two basin boundaries, $x = 0.4$ and $x = 0.16$. In particular, at $n = 603$ the map enters the basin of B, but it is not attracted to B. Instead, it jumps into the basin of A immediately in its next iteration and is staying on A in the following evolution. The results in Fig. 3(b) show again that basin crossing is a necessary but not sufficient condition for map transition. Still, the basin transition can be understood from the competition between the map function and the coupling perturbations.

The similar process of interface collision is also observed when the interfaces of the C and A cluster collide. In Fig. 3(c), we plot the trajectory of the 46th map during the process of interface collision [around $n' = 300$ in Fig. 1(a), as marked by the upper rectangle]. It is seen that after crossing the basin boundaries thrice, the map is finally stabilized to B. That is, with the vanishing of the A cluster, a B cluster is newly generated, which, in the following evolution, will be gradually expanded by consuming the C cluster.

Combining the results of Figs. 2 and 3, we get the following properties for the cyclic pattern in Fig. 1(a). First, the pattern evolution is governed by the competitions of three synchronous clusters. Except the points where cluster interfaces collide, at any instant of the system evolution there always exist two synchronous clusters. Second, for the given pair of competing clusters, the cluster interface is of fixed width and is moving with a constant speed. Third, the newly born cluster, as appeared after the collision of the two counterpropagating cluster interfaces, is generated by the fixed order; i.e., the vanishing of the A, B, and C clusters gives rise to, respectively, the births of the B, C, and A clusters. Finally, the system dynamics returns to exactly the same pattern after a fixed number of iterations; i.e., the cyclic pattern has the period $T = 888$.

C. Pattern sensitivity

We now investigate the sensitivity feature of the cyclic pattern. Since the maps are identical and are coupled on a ring-structure network, the transient process of the system evolution is solely determined by the map initial conditions. A close look at Fig. 1(b) shows that, after about 20 iterations, there are three synchronous clusters formed in the system. This configuration of the synchronous cluster is very different from that of Fig. 1(a) (where only two clusters are generated after the transient process), which results in the different pattern evolution. In particular, due to the cyclical competitions among the three clusters, a traveling synchronous pattern is formed in this case. As discussed above, the evolution of the cyclic pattern relies on the competition of only two clusters (so as to make the cluster interfaces collide), any transient process failing in generating two synchronous clusters will be not able to produce the cyclic pattern. This feature of cluster-configuration-induced pattern sensitivity is further exemplified by the results presented in Fig. 4(a). In plotting Fig. 4(a), we set

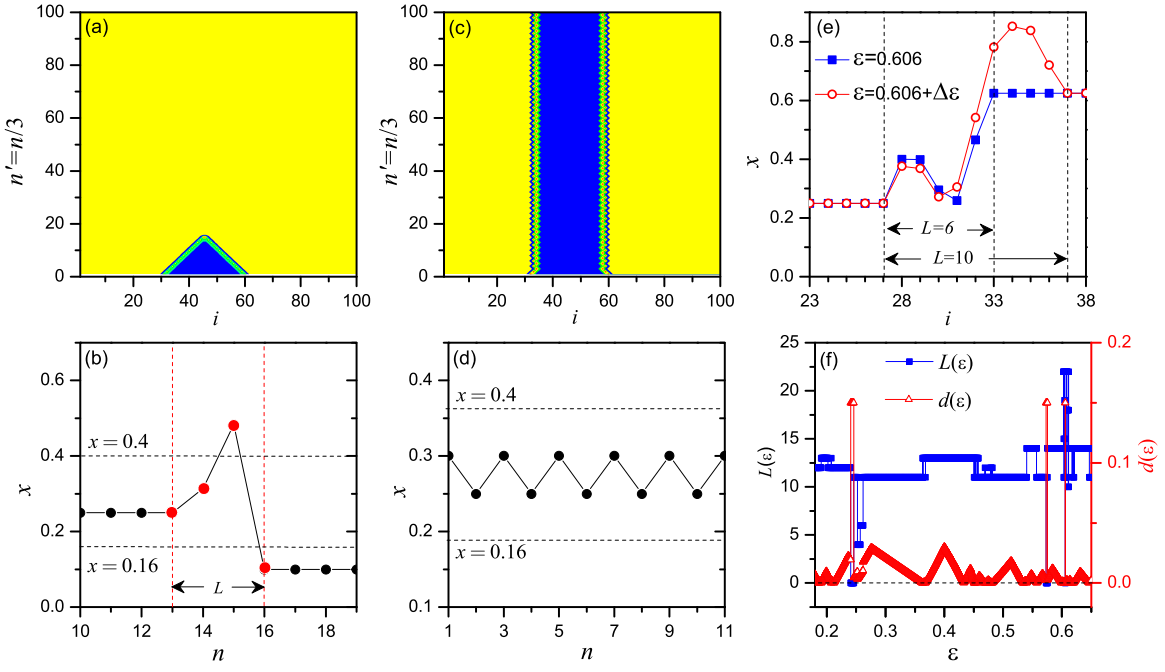

FIG. 4. (Color online) The sensitivity of the cyclic pattern to the map initial conditions (a, b) and the coupling strength (c–f). The initial conditions are artificially arranged, with A for $i \in [31,60]$ and C for the remaining maps. By the same coupling strength used in Fig. 1, (a) the pattern evolution and (b) the trajectory of the 46th map. By changing the coupling strength to $\varepsilon = 0.36$, (c) the formation of stationary synchronous pattern and (d) the trajectory of the 35th map located at the end of the left-side interface. (e) The sensitivity of the cluster interface to the coupling strength. For $\varepsilon = 0.606$, $L = 6$ (filled squares); for $\varepsilon = 0.606 + \Delta\varepsilon$, $L = 11$ (open circles), where $\Delta\varepsilon = 1 \times 10^{-5}$. (f) The variations of the interface width (left scale, filled squares), L, and the boundary distance (right scale, open triangles), d, as a function of the coupling strength. It is seen that the value of L is only adjusted at the points of $d \approx 0$.

artificially the initial condition as A for maps $i \in [31,60]$ and C for the remaining maps in the lattice. This configuration is very close to the cyclic pattern at the moment $n' = 283$ [Fig. 1(a)], except that here the A cluster contains one more map. In Fig. 4(a) it is seen that, after the collision of the interfaces, the A cluster completely disappears (no new cluster is generated) and the system reaches the state of global synchronization. The trajectory of the 46th map, which is one of the two central maps in the A cluster, is plotted in Fig. 4(b). It is seen that this trajectory is significantly different from that of Fig. 3(c). Specifically, in Fig. 3(c) the map is attracted to B after the collision, while in Fig. 4(b) the map is attracted to C.

The cyclic pattern is also sensitive to the coupling strength. By the same initial conditions used in Fig. 4(a), we plot in Fig. 4(c) the system evolution under the coupling strength $\varepsilon = 0.36$. It is seen that this time the interfaces are pinned on the lattice and the contents of the clusters do not change with time; i.e., the system is developed into a stationary synchronous pattern. To have more details on the dynamics of the cluster interface for this case, we plot in Fig. 4(d) the trajectory of the 35th map, which is located at the left-side interface. It is shown that during the process of system evolution, the trajectory is oscillating periodically within the same basin; i.e., no basin crossing is observed. To characterize further the sensitive dependence of the synchronous pattern on the coupling strength, we plot in Fig. 4(e) the interfaces generated by two coupling strengths of a tiny difference, $\Delta\varepsilon = 1 \times 10^{-5}$. It is seen that, with such a small difference of the coupling strength, the cluster interface is significantly changed; e.g., the interface width is changed from $L = 6$ to 10.

Considering the fact that the isolated map has the superstable period-three orbit, it is somewhat surprising to see in Fig. 4(e) that the cluster interface is so sensitive to the coupling strength (in systems of coupled periodic oscillators, the interface of homogeneous phases is normally not sensitive to the coupling strength, e.g., the kink and antikink patterns [36,37]). To check out the nature of this sensitivity, we plot in Fig. 4(f) the variation of the interface width, L, as a function of ε. Interestingly, it is found that as ε varies, L is jumping randomly among different plateaus. More specifically, the parameter space is divided into intervals of different sizes, and the width of the cluster interface is keeping unchanged within each interval. Figure 4(f) thus suggests that the cluster interface (synchronous patterns) is sensitive only at some critical coupling strengths, e.g., the one used in Fig. 4(e), while for the general coupling strength, the interface (synchronous pattern) is still stable.

What happens at the critical coupling strengths? Noticing the crucial role of basin crossing in determining the map transition (see the results in Figs. 2 and 3), it is natural to link the critical couplings to the events of basin crossing. To verify this, we measure the minimum distance of the maps in the interface to the basin boundaries and study how this distance is varying with ε. The boundary distance is defined as $d = min|x_j - x_k^b|$, with $j = 1, \ldots, L$ the states of the maps in the cluster interface, and x_k^b, with $k = 1,2,3$, the basin boundaries. Roughly, d measures the propensity that a map in the interface is going to escape from its original basin. The smaller is d, the higher is the possibility for the interface to be adjusted. In this sense, the interface is expected to be dramatically modified at the points $d \approx 0$. This is indeed what we observe in Fig. 4(f), where it is shown that L is adjusted at exactly the points of $d \approx 0$.

It is worth mentioning that, while we attribute the pattern sensitivity to the crossing of the map trajectory with the basin boundaries, it is difficult to predict when will this crossing occur, i.e., the points where $d \approx 0$ in Fig. 4(f), and what the new interface looks like. This is partially due to the high nonlinearity of the local map (the existence of the discontinuous point) and also for the reason that the width of the interface is not fixed. As shown in Fig. 4(f), both the width and height of the plateaus seem to be randomly varying.

IV. PATTERN CONTROL

By the sensitivity feature of cyclic pattern, we are able to alter or control the system dynamics in a more efficient manner. As discussed above, a distinct feature of the piecewise-linear map is the continuous basin distribution of the fixed points, which makes the map transition crucially dependent on the event of basin crossing. If during the process of pattern evolution some maps are slightly perturbed, randomly or intentionally, in such a way that a new event of basin crossing occurs, then it might be possible for the perturbed maps to be transferred to a new cluster, and resulting in the generation of a new pattern. This idea of perturbation-induced pattern alteration is verified by numerical simulations. In Fig. 5(a) we add small-amplitude random perturbations [independent and identically distributed random variables within the range $(0,1 \times 10^{-2})$] to the cyclic pattern shown in Fig. 1(a) and

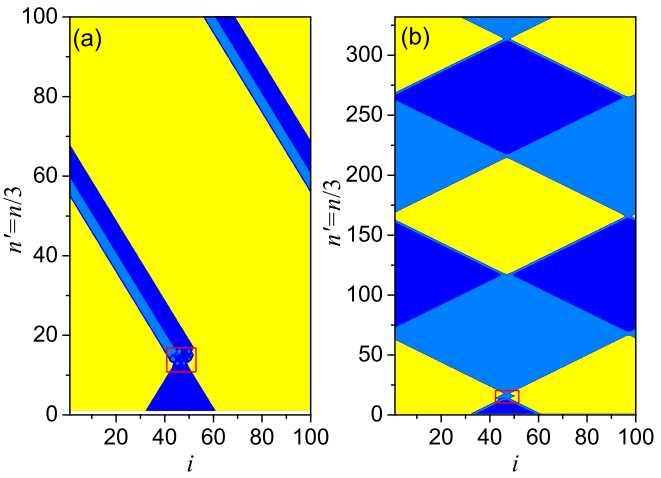

FIG. 5. (Color online) (a) The alteration of cyclic pattern by small random perturbations. The system parameters and initial conditions are the same as Fig. 1(a). The random perturbations, of the amplitude 1×10^{-2}, are added to maps $42 \leqslant i \leqslant 52$ from $n = 39$ to 45, as marked by the rectangle. The system dynamics is switched from a cyclic to traveling pattern. (b) The generation of a cyclic pattern by the method of pinning control. The system parameters and initial conditions are the same as Fig. 4(a). The pinning signals are added on only two maps, $l = 45,46$, and sustained from $n = 50$ to 55, as marked by the rectangle. The pinning strength is $\eta = 0.2$, and the targeting trajectory is chosen as the orbit of the B cluster. The system, which is originally developed to global synchronization, is now controlled to the cyclic pattern shown in Fig. 1(a).

plot the time evolution of the system. The perturbations are added on the maps $42 \leqslant i \leqslant 52$ and sustained for only a short period (from $n = 39$ to 45). It is seen that, after the random perturbations, the cyclic pattern is altered to a traveling pattern.

While by random perturbations the synchronous pattern can be conveniently modified, the new pattern is generated in an uncontrollable manner. For instance, if we extend the period of random perturbations to $n = 80$ in Fig. 5(a), the system will finally reach the state of global synchronization. In many practical applications, the system dynamics needs to be controlled precisely to some predefined patterns. In such a case, the use of some control techniques are necessary. Here we adopt the method of pinning control (a method that has been widely used in controlling spatiotemporal chaos [51,52]) and investigate how cyclic pattern can be induced from global synchronization. To demonstrate, we use the pattern shown in Fig. 4(a) as the reference and choose the cyclic pattern in Fig. 1(a) as the target. In our simulations, we add pinning signals to only two neighboring maps in the lattice, $l = 45,46$ [the central maps of the A cluster in Fig. 4(a)], and "pulling" them to some predefined trajectories. Specifically, the dynamics of the pinned maps reads

$$x_l(n+1) = (1-\varepsilon) f(x_l(n)) + \frac{\varepsilon}{2}[f(x_{l+1}(n)) + f(x_{l-1}(n))] + \eta[f(x^s(n)) - f(x_l(n)], \quad (4)$$

where η represents the pinning strength, and $x^s(n)$ denotes the targeting trajectory to which the maps are going to be controlled. Here, to achieve the cyclic pattern shown in Fig. 1(a), $x^s(n)$ is chosen as the orbit of the B cluster. The control is started at $n = 50$ and stopped at $n = 55$. The results are presented in Fig. 5(b). It is seen that, instead of being absorbed into the C cluster, the pinned maps are successfully transferred to B, forming a small-size B cluster. After that, the system evolution follows exactly the same pattern shown in Fig. 1(a).

V. DISCUSSION AND CONCLUSION

Can cyclic synchronous patterns be observed in other systems, e.g., when the map dynamics is changed? To address this question, we change the lattice model by (1) employing high-periodic orbits and (2) using a different map function, and searching for the cyclic patterns. Setting $b = 0.05$ in Eq. (2), the trajectory of the isolated map will be changed to a superstable period-four orbit: $x_1^* = b = A'$, $x_2^* = ab = B'$, $x_3^* = a^2 b = C'$, and $x_4^* = ab^3 = D'$. Using this period-four orbit as the local dynamics, we simulate again the system evolution according to Eq. (1). By the coupling strength $\varepsilon = 0.048$ and using a set of random initial conditions, we plot in Fig. 6(a) the system evolution as a function of time. It is seen that after a transient period about $n = 1.5 \times 10^3$ iterations, the system is also stabilized onto a cyclic pattern. Comparing to the case of period-three maps, it is seen that the cyclic pattern is clearly complicated. More specifically, the cyclic pattern is sustained by the competitions of four synchronous clusters, and the pattern period is significantly increased ($T = 2.411 \times 10^3$). However, the clusters are still consumed by a fixed, cyclic order (A' cluster $\rightarrow$ B' cluster $\rightarrow$ C' cluster $\rightarrow$ D' cluster), and new clusters are generated by the collision

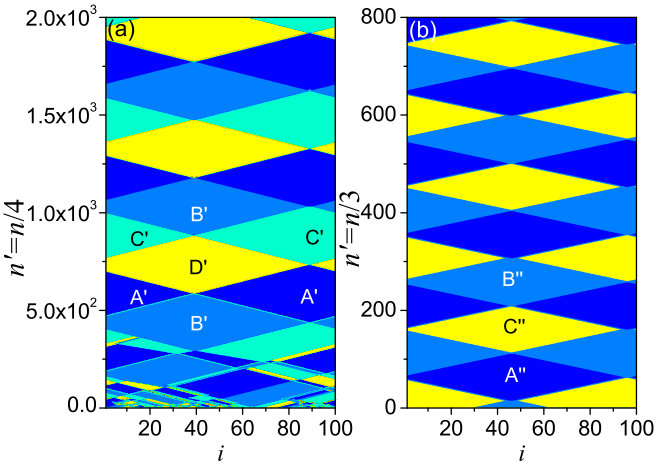

FIG. 6. (Color online) Cyclic synchronous patterns generated in the lattices of coupled (a) period-four maps and (b) new maps described by Eq. (5). (a) $\varepsilon = 0.048$, $T = 2.411 \times 10^3$. (b) $\varepsilon = 0.03$, $T = 875$.

of counterpropagating cluster interfaces (the vanishing of the A', B', C', and D' clusters leads to, respectively, the births of the C', D', A', and B' clusters). Like the case of period-three map, the cyclic pattern is also sensitive to the the map initial conditions and the coupling strength (not shown). The similar cyclic patterns are also observed in even higher period orbits, which can be realized by decreasing the parameter b in Eq. (2). The general finding is that the higher the periodicity of the orbit, the lower the possibility to generate the cyclic pattern from a set of randomly chosen initial conditions. For instance, for the period-16 map ($b = 0.01$), no cyclic pattern is observed in 1×10^3 realizations.

Cyclic synchronous pattern can be also generated in other types of discontinuous maps. Replacing the map function with

$$f(x) = \begin{cases} a'x + (1-a'), & x \in [0,c') \\ b'x, & x \in [c',1], \end{cases} \quad (5)$$

we simulate the system evolution under different initial conditions and coupling strengths. This map is another typical model of discontinuous system, which has been extensively studied in the literature [53]. By the parameters $(a',b',c') = (0.7,0.2,0.4)$, the isolated map has a superstable period-three orbit ($x_1'' \approx 0.11 = A''$,$x_2'' \approx 0.38 = B''$, and $x_3'' \approx 0.57 = C''$). Using this period-three orbit as the local dynamics, we plot in Fig. 6(b) the system evolution under the coupling strength $\varepsilon = 0.03$. It is seen that the system evolution is stabilized onto a cyclic pattern very similar to that of Fig. 1(a), including the number of clusters, the competition relationship among the clusters, and the generation of new clusters after the interface collisions. Still, the cyclic pattern is found as sensitive to the initial conditions and coupling strength.

The above results are in accordance with expectations, as the underlying mechanisms of the map transition, namely, the continuous basin distribution and basin crossing, are still valid in these two cases. Specifically, given the coupling perturbation is larger enough, the map trajectory will be able to cross the basin boundaries, making it possible to transfer the maps between different clusters. Furthermore, if a new cluster

is generated after the collision of two counterpropagating cluster interfaces, then the processes of cluster competition and interface collisions will be continued; i.e., a cyclic pattern will be formed. From this reasoning, it is our conjecture that, given the basins of the map attractors are continuously distributed, cyclic synchronous patterns are always observable through turning the coupling strength or the system initial conditions. Although our conjecture is based on the simple model of piecewise-linear maps, we expect the similar cyclic patterns can be generated in the general discontinuous systems, e.g., piecewise-linear maps with more discontinuous points.

It is worth noting that the synchronous patterns we have observed cannot be completely explained by the generic Hopf bifurcation. In the general scenario of Hopf bifurcation, the breaking of circular $\mathbb{O}(2)$ symmetry will lead to patterns of strict symmetries, i.e., standing waves of spatial (k-fold) symmetry and traveling waves of equivalent phase shift [54]. These symmetries, however, are broken in the synchronous patterns observed in the present work. Specifically, in the stationary and traveling synchronous patterns, it is seen that the size of the synchronous clusters is uneven and sensitive to the initial conditions [e.g., Fig. 1(b)]; and in the cyclic synchronous patterns, it is seen that at any instant of the pattern evolution there are always missed states of the periodic orbit [e.g., Fig. 1(a)]. Noticing that the dynamics of discontinuous systems is also governed by the boundary collision (BC) bifurcation [55], we thus speculate that the asymmetric feature of synchronous patterns is rooted in the interaction of BC and Hopf bifurcations; i.e., it belongs to a codimension-2 bifurcation [54]. The occurrence of BC bifurcation is evidenced in Fig. 4(f), where it is shown that the interface width is adjusted at exactly the points where the boundary distance reaches zero. According to the mechanism of mode interactions, when two distinct types of bifurcation coincide in the parameter space, the $\mathbb{O}(2)$ symmetry will be broken in new ways, resulting in new forms of patterns not presented in Hopf bifurcation. The Thomist approach [54] suggests that, to analyze this type of pattern, it is necessary to unfold the mode interaction by an additional parameter, a topic worthy of further studies.

In summary, we have studied the collective behaviors in the lattices of coupled piecewise-linear maps and found a new type of pattern: the cyclic synchronous pattern. We have conducted a detail analysis on the properties of this new pattern and analyzed its underlying mechanisms from the viewpoint of dynamics competition. The sensitivity properties of the cyclic pattern also have been explored, based on which two new approaches have been proposed for altering and controlling the patterns. The findings enrich our knowledge of synchronization dynamics in coupled complex systems and might helpful in understanding the functioning of some realistic systems [1–5].

ACKNOWLEDGMENTS

This work was supported by the National Natural Science Foundation of China under Grant Nos. 10875076 and 11375109. This work is also supported by the Fundamental Research Funds for the Central Universities under Grant No. GK201303002 and the Interdisciplinary Project of Shaanxi Normal University under Project No. 5.

[1] E. R. Kandel, J. H. Schwartz, and T. M. Jessell, *Principles of Neural Science* (McGraw-Hill, New York, 2000).
[2] W. Dement and N. Kleitman, Cyclic variations in EEG during sleep and their relation to eye movements, body motility, and dreaming, Electroencephal. Clin. Neurophysiol. **9**, 673 (1957).
[3] H. Cruse, What mechanisms coordinate leg movement in walking arthropods? Trends Neurosci. **13**, 15 (1990).
[4] P. Maquet, The role of sleep in learning and memory, Science **294**, 1048 (2001).
[5] P. Arena, L. Fortuna, and M. Branciforte, Reaction-diffusion CNN algorithms to generate and control artificial locomotion, IEEE Trans. Circuits Sys. I **46**, 253 (1999).
[6] S. H. Strogatz, Human sleep and circadian rhythms: a simple model based on two coupled oscillators, J. Math. Biol. **25**, 327 (1987).
[7] T. Zielinska, Coupled oscillators utilised as gait rhythm generators of a two-legged walking machine, Biol. Cybern. **74**, 263 (1996).
[8] H. Cruse, T. Kindermann, M. Schumm, J. Dean, and J. Schmitz, Walknet-a biologically inspired network to control six-legged walking, Neural Netw. **11**, 1435 (1998).
[9] S. Roy, J. M. Krueger, D. M. Rector, and Y. Wan, A. network model for activity-dependent sleep regulation, J. Theor. Biol. **253**, 462 (2008).
[10] R. Ma, J. Wang, and Z. Liu, Robust features of chimera states and the implementation of alternating chimera states, Europhys. Lett. **91**, 40006 (2010).
[11] I. Z. Kiss, C. G. Rusin, H. Kori, and J. L. Hudson, Engineering complex dynamical structures: Sequential patterns and desynchronization, Science **316**, 1886 (2007).
[12] C. Fu, Z. Deng, L. Huang, and X. G. Wang, Topological control of synchronous patterns in systems of networked chaotic oscillators, Phys. Rev. E **87**, 032909 (2013).
[13] C. Fu, W. Lin, L. Huang, and X. G. Wang, Synchronization transition in networked chaotic oscillators: The viewpoint from partial synchronization, Phys. Rev. E **89**, 052908 (2014).
[14] Y. Kuramoto, *Chemical Oscillations, Waves and Turbulence* (Springer-Verlag, Berlin, 1984).
[15] A. S. Pikovsky, M. G. Rosenblum, and J. Kurths, *Synchronization: A Universal Concept in Nonlinear Science* (Cambridge University Press, Cambridge, 2001).
[16] S. Strogatz, *Sync: The Emerging Science of Spontaneous Order* (Hyperion, New York, 2003).
[17] S. Boccaletti, V. Latora, Y. Moreno, M. Chavez, and D.-U. Hwang, Complex networks: Structure and dynamics, Phys. Rep. **424**, 175 (2006).
[18] D. J. Watts and S. H. Strogatz, Collective dynamics of 'small-world' networks, Nature (London) **393**, 440 (1998).
[19] A.-L. Barabási and R. Albert, Emergence of scaling in random networks, Science **286**, 509 (1999).
[20] T. Nishikawa, A. E. Motter, Y.-C. Lai, and F. C. Hoppensteadt, Heterogeneity in oscillator networks: are smaller worlds easier to synchronize? Phys. Rev. Lett. **91**, 014101 (2003).

[21] A. E. Motter, C. Zhou, and J. Kurths, Weighted networks are more synchronizable: How and why, AIP Conf. Proc. **776**, 201 (2005).
[22] X. G. Wang, Y.-C. Lai, and C. H. Lai, Enhancing synchronization based on complex gradient networks, Phys. Rev. E **75**, 056205 (2007).
[23] A. Arenas, A. Diaz-Guilera, J. Kurths, Y. Moreno, and C. Zhou, Synchronization in complex networks, Phys. Rep. **469**, 93 (2008).
[24] J. F. Heagy, L. M. Pecora, and T. L. Carroll, Short wavelength bifurcations and size instabilities in coupled oscillator systems, Phys. Rev. Lett. **74**, 4185 (1995).
[25] G. Hu, Y. Zhang, H. A. Cerdeira, and S. Chen, From low-dimensional synchronous chaos to high-dimensional desynchronous spatiotemporal chaos in coupled systems, Phys. Rev. Lett. **85**, 3377 (2000).
[26] Y. Zhang, G. Hu, H. A. Cerdeira, S. Chen, T. Braun, and Y. Yao, Partial synchronization and spontaneous spatial ordering in coupled chaotic systems, Phys. Rev. E **63**, 026211 (2001).
[27] B. Ao and Z. G. Zheng, Partial synchronization on complex networks, Europhys. Lett. **74**, 229 (2006).
[28] X. G. Wang, S. Guan, Y.-C. Lai, B. Li, and C. H. Lai, Desynchronization and on-off intermittency in complex networks, Europhys. Lett. **88**, 28001 (2009).
[29] C. Fu, H. Zhang, M. Zhan, and X. G. Wang, Synchronous patterns in complex systems, Phys. Rev. E **85**, 066208 (2012).
[30] L. M. Pecora, F. Sorrentino, A. M. Hagerstrom, T. E. Murphy, and R. Roy, Cluster synchronization and isolated desynchronization in complex networks with symmetries, Nat. Commun. **5**, 4079 (2014).
[31] J. Gómez-Gardeñes, Y. Moreno, and A. Arenas, Paths to synchronization on complex networks, Phys. Rev. Lett. **98**, 034101 (2007).
[32] K. Kaneko, *Theory and Application of Coupled Map Lattices* (Wiley, Chichester, 1993).
[33] K. Kaneko, Clustering, coding, switching, hierarchical ordering, and control in network of chaotic elements, Physica D **41**, 137 (1990).
[34] M. Hasler, Yu. Maistrenko, and O. Popovych, Simple example of partial synchronization of chaotic systems, Phys. Rev. E **58**, 6843 (1998).
[35] F. H. Willeboordse, Hints for universality in coupled map lattices, Phys. Rev. E **65**, 026202 (2002).
[36] K. Kaneko, Period-doubling of kink-antikink patterns, quasi-periodicity in antiferro-like structures and spatial intermittency in coupled map lattices, Prog. Theor. Phys. **72**, 480 (1984).
[37] W. Liu, Y. Wu, W. Zou, J. Xiao, and M. Zhan, Pattern with kinks and pulses in coupled periodic map lattices, Phys. Rev. E **76**, 036215 (2007).
[38] K. Kaneko, Global traveling wave triggered by local phase slips, Phys. Rev. Lett. **69**, 905 (1992).
[39] R. Kapral, R. Livi, G.-L. Oppo, and A. Politi, Dynamics of complex interfaces, Phys. Rev. E **49**, 2009 (1994).
[40] R. Carretero-González, D. K. Arrowsmith, and F. Vivaldi, Topological invariants in Fermi systems with time-reversal invariance, Phys. Rev. E **61**, 1329 (2000).
[41] P. M. Gade, D. V. Senthilkumar, S. Barve, and S. Sinha, Power-law persistence characterizes traveling waves in coupled circle maps with repulsive coupling, Phys. Rev. E **75**, 066208 (2007).
[42] M. Bauer, S. Habip, D. R. He, and W. Martienssen, New type of intermittency in discontinuous maps, Phys. Rev. Lett. **68**, 1625 (1992).
[43] S. X. Qu, B. Christiansen, and D. R. He, Hole-induced crisis in a piece-wise linear map, Phys. Lett. A **201**, 413 (1995).
[44] S. X. Qu, S. G. Wu, and D. R. He, Multiple devil's staircase and type-V intermittency, Phys. Rev. E **57**, 402 (1998).
[45] S. X. Qu, Y. Z. Lu, L. Zhang, and D. R. He, Discontinuous bifurcation and coexistence of attractors in a piecewise-linear map with a gap, Chin. Phys. B **17**, 4418 (2008).
[46] R. F. Pereira, R. L. Viana, S. R. Lopes, M. C. Vergès, and S. E. de Pinto, Parametric evolution of unstable dimension variability in coupled piecewise-linear chaotic maps, Phys. Rev. E **83**, 037201 (2011).
[47] H. L. Zou, S. G. Guan, and C. H. Lai, Dynamical formation of stable irregular transients in discontinuous map systems, Phys. Rev. E **80**, 046214 (2009).
[48] A. Polynikis, M. di Bernardo, and S. J. Hogan, Synchronizability of coupled PWL maps, Chaos Solitons Fractals **41**, 1353 (2009).
[49] R. Kapral, R. Livi, and A. Politi, Critical behavior of complex interfaces, Phys. Rev. Lett. **79**, 2277 (1997).
[50] J. Mo, Y. Li, C. Wei, M. Yang, H. Gu, S. Qu, and W. Ren, Interpreting a period-adding bifurcation scenario in neural bursting patterns using border-collision bifurcation in a discontinuous map of a slow control variable, Chin. Phys. B **19**, 080513 (2010).
[51] G. Hu and Z. Qu, Controlling spatiotemporal chaos in coupled map lattice systems, Phys. Rev. Lett. **72**, 68 (1994).
[52] P. Liu, Z. Deng, L. Yang, M. Zhan, and X. G. Wang, Network approach to the pinning control of drift-wave turbulence, Phys. Rev. E **89**, 062918 (2014).
[53] G. I. Bischi, L. Gardini, and F. Tramontana, Bifurcation curves in discontinuous maps, Discrete Contin. Dyn. Syst. Ser. B **13**, 249 (2010).
[54] M. Golubitsky and I. Stewart, Recent advances in symmetric and network dynamics, Chaos **25**, 097612 (2015).
[55] H. E. Nusse, E. Ott, and J. A. Yorke, Border-collision bifurcations: An explanation for observed bifurcation phenomena, Phys. Rev. E **49**, 1073 (1994).